

Typical X-ray Outburst Light Curves of Aql X-1*

ÖMER FARUK ÇOBAN ¹ AND ÜNAL ERTAN ¹

¹*Faculty of Engineering and Natural Sciences, Sabancı University
Orhanlı, Tuzla 34956, İstanbul, Türkiye*

ABSTRACT

We show that a typical X-ray outburst light curve of Aql X-1 can be reproduced by accretion onto the neutron star in the frame of the disk instability model without invoking partial accretion or propeller effect. The knee and the subsequent sharp decay in the X-ray light curve can be generated naturally by taking into account the weak dependence of the disk aspect ratio, h/r , on the disk mass-flow rate, \dot{M}_{in} , in the X-ray irradiation flux calculation. This \dot{M}_{in} dependence of h/r only slightly modifies the irradiation temperature profile along the hot disk in comparison to that obtained with constant h/r . Nevertheless, this small difference has a significant cumulative effect on the hot disk radius leading to a much faster decrease in the size of the hot disk, and thereby to a sharper decay in the X-ray outburst light curve. The same model also produces the long-term evolution of the source consistently with its observed outburst recurrence times and typical light curves of Aql X-1. Our results imply that the source accretes matter from the disk in the quiescent state as well. We also estimate that the dipole moment of the source $\mu \lesssim 4 \times 10^{26} \text{ G cm}^3$ ($B \lesssim 4 \times 10^8 \text{ G}$ at the surface).

Keywords: Accretion, Accretion disks — Stars: neutron — X-rays: binaries — X-rays: bursts

1. INTRODUCTION

Low-mass X-ray binaries (LMXBs) are systems containing either a neutron star (NS) or a black hole (BH) and a low-mass companion star with mass $M < 1M_{\odot}$. In LMXBs, mass is transferred from the companion to the compact object through Roche-lobe overflow. Due to its angular momentum, the matter cannot fall directly onto the star. Instead, the material forms a geometrically thin accretion disk around the NS (Frank et al. 2002). The matter in the disk moves in Keplerian orbits with speed $v_K = (GM/r)^{1/2}$ where G is the gravitational constant, M is the mass of the NS, and r is the radial distance from the center. Through viscous processes, angular momentum is carried outwards while the matter flows inwards toward the compact object.

A small fraction of these systems are persistent X-ray sources, while the remaining larger fraction consists of transient systems, with both neutron stars (NSXTs) and black holes (BHXTs) that show X-ray outbursts with large ranges of recurrence and duration time-scales (see e.g. Psaltis 2006). The inner disk in NSXTs is cut at a radius, r_{in} , depending on the mass-flow rate,

\dot{M}_{in} , of the disk and the dipole moment $\mu = BR_*^3$ of the NS, where B and R_* are the dipole field strength at the equator and the radius of the star respectively. At the co-rotation radius $r_{\text{co}} = (GM/\Omega_*^2)^{1/3}$, the angular speed of the NS, Ω_* , equals the Keplerian angular speed, Ω_K , of the disk matter. If $r_{\text{in}} \leq r_{\text{co}}$, the matter can flow from the inner disk along the closed field lines onto the NS. In the case that $r_{\text{in}} > r_{\text{co}}$ the matter is estimated to be thrown out from the inner disk (propeller effect; Illarionov & Sunyaev 1975). For a given μ , the critical \dot{M}_{in} level for the onset of the propeller mechanism is not well known. For spherical accretion onto a non-rotating magnetized star, magnetic pressure balances the ram pressure of the inflowing matter at Alfvén radius, $r_A \simeq (GM)^{-1/7} \mu^{4/7} \dot{M}_{\text{in}}^{-2/7}$ (Davidson & Ostriker 1973; Lamb et al. 1973). In the case of disk accretion, r_{in} is conventionally estimated by equating the viscous and magnetic stresses and found to be $r_{\xi} = \xi r_A$ with $\sim 0.5 < \xi < 1$ (Ghosh & Lamb 1979; Kluźniak & Rappaport 2007).

It was proposed that there is a minimum critical X-ray luminosity, L_X , for a persistent LMXB such that the entire disk is kept hot above the hydrogen ionization temperature by the X-ray irradiation flux with an L_X above this critical level (van Paradijs 1996). When

* Accepted for publication in The Astrophysical Journal (ApJ)

L_X decrease below the critical rate, the outer cold regions of the disk enter a low viscosity state with an inefficient mass transfer from the outer to the inner disk with a rate lower than the mass-flow rate, \dot{M}_c , from the companion to the outer disk. This leads to a gradual increase in the surface densities and temperatures of the outer disk. When the outer disk temperature exceeds the critical level at a radius, a heating front propagates to inner and outer radii, which could take most of the disk into the "hot state" with higher viscosities enhancing the mass transfer to the inner disk. The resultant abrupt increase in \dot{M}_{in} at the inner disk is observed as an X-ray outburst. In the outburst phase, efficient mass transfer from the outer radii decreases the surface densities and temperatures of the outer disk. Eventually, starting from the outer disk, propagation of a cooling front inward could take the entire disk into the "cold state" with much lower \dot{M}_{in} and L_X (quiescent state). To sum up, the outer disk behaves like a mass reservoir in the quiescent state, and this mass is released as a result of thermal-viscous disk instability producing an X-ray outburst (see e.g. Lasota 2001; Frank et al. 2002 for details).

The L_X peak in outbursts and the recurrence time-scale, τ_{rec} , depend on the size of the disk together with the mass transfer rate from the companion, as well as the X-ray irradiation strength during the outburst. The X-ray irradiation slows down the inward propagation of the cooling front during the outburst state. Therefore, the outer disk of a system with relatively high L_X is evacuated more efficiently during outbursts, which needs a longer τ_{rec} to refill the disk. For instance, τ_{rec} is of the order of weeks for dwarf novae (DNs), while for NSXTs and BHXTs τ_{rec} varies from months to decades (Frank et al. 2002).

In the disk instability models (DIMs), the disk diffusion equation is usually solved using the α -prescription of the kinematic viscosity $\nu = \alpha c_s h$ (Shakura & Sunyaev 1973), where c_s is the sound speed and h is the pressure scale-height of the disk. The basic characteristics of DN light curves can be reproduced with $\alpha_h \simeq 0.1$ and $\alpha_c \simeq 0.01 - 0.05$ for the hot and cold viscosity states, respectively. DIMs can also account for the outburst light curves and recurrence times of transient LMXBs with α_h and α_c values similar to those used for DNs, provided that the effect of X-ray irradiation on the disk dynamics during the outburst states is included in the models (King 1998; King & Ritter 1998; Dubus et al. 1999, 2001).

A characteristic "knee" followed by a steepening in the X-ray outburst light curves observed from a variety of magnetized stars in binaries including some NSXTs was

proposed to be the signature of the onset of the propeller effect at a critical L_X corresponding to $r_\xi = \xi r_A = r_{co}$ with $\xi \simeq 0.5$ (Zhang et al. 1998; Campana et al. 1998, 2018). Among these NSXTs, Aql X-1 is a prototypical source with a spin period of $P = 1.8$ ms (Casella et al. 2008), accreting matter from a K-type companion. The source exhibits outbursts with a recurrence time $\tau_{rec} \sim 1$ yr. Güngör et al. (2014) classified these outbursts into three types based on their duration and peak flux. Among these, the 2010 outburst belongs to the most common type. During these outbursts, the L_X peak exceeds 10^{37} erg s $^{-1}$ within a few days (Campana et al. 2013). After the peak, the X-ray light curve displays a smooth and slow exponential decay lasting for a few weeks, followed by a sharp turn downward, forming a knee-like morphology at an L_X level of a few 10^{36} erg s $^{-1}$. Subsequently, L_X decreases more steeply to the quiescent level within several days (Campana et al. 2014).

A steepening of the X-ray light curve during the decay phase is a behavior estimated in the DIM resulting from the inward propagation of the cooling front (see e.g. King & Ritter 1998). Recently, Lipunova et al. (2022) showed through detailed numerical analysis that the knee in the decay curve of Aql X-1 could be produced as a result of the shrinking size of the hot inner disk during the decay phase of the outburst. Initially, the X-ray light curve is similar to that of a purely viscous relaxation (without disk instability). The presence of a cold-hot border is communicated to the innermost disk after a viscous time across the hot inner disk. While r_h is decreasing, the viscous time-scale of the hot disk also decreases. Below a critical level, this leads to a steeper \dot{M}_{in} and L_X decay compared to those in purely viscous decay. This sequence of events governed by the dynamics and viscous time-scale of the inner hot disk causes a transition from a slower to a faster decay in L_X , producing a knee-like morphology in the X-ray outburst light curve. Lipunova et al. (2022) modeled the X-ray outburst light curve of Aql X-1 with different assumptions (partial accretion, strong propeller, and total accretion). They obtain reasonable results with both the total accretion and partial accretion assumptions. For the total accretion case, they assumed that all the inflowing disk matter is accreted onto the star including the $r_{in} > r_{co}$ epoch. They calculate the total L_X including both accretion and disk luminosity, while L_{disc} is dominating L_X . During the decay phase, r_{in} is increasing with decreasing \dot{M}_{in} . The effect of this outward propagation of the inner disk on the sharpening of the decay curve after the knee is not clear. Lipunova et al. (2022) pointed out

that the \dot{M}_{in} dependence of the h/r ratio is significant in reproducing the sharper decay curve.

In this work, we also investigate the X-ray outburst light curves of Aql X-1 together with its recurrence characteristics in the frame of DIMs. In our model, the physical reason for the formation of the knee is similar to that found by Lipunova et al. (2022). Taking the \dot{M}_{in} dependence of the disk aspect ratio into account in the X-ray irradiation flux calculations, we demonstrate that the light curve morphology of Aql X-1 can be reproduced by the accretion luminosity without including partial accretion or a strong propeller in the model. As pointed out by Lipunova et al. (2022), we also find that the weak \dot{M}_{in} dependence of the disk aspect ratio significantly affects the decay morphology of the light curve. Furthermore, this model also reproduces the long-term characteristics of the recurrent outbursts of Aql X-1. The X-ray outburst light curves, the quiescent L_X level, and the recurrence time produced in the model are in good agreement with the observations. In section 2, we describe our model briefly. We discuss the results of the model calculations in section 3 and summarize our conclusions in section 4.

2. MODEL

We use the numerical code employed earlier by Ertan & Alpar (2002) to simulate the fast-rise-exponential-decay (FRED) type outburst light curves of BHXTs. Here, we briefly describe the model calculations.

We represent the mass distribution of the disk before the X-ray outburst with a Gaussian surface density distribution $\Sigma(r, t = 0) = \Sigma_0 \exp[-\{(r - r_{\text{circ}}/\Delta r)\}^2]$ centered at the circularisation radius, r_{circ} . Through numerical calculations, we solve the diffusion equation

$$\frac{\partial \Sigma}{\partial t} = \frac{3}{r} \frac{\partial}{\partial r} \left[r^{1/2} \frac{\partial}{\partial r} (\nu \Sigma r^{1/2}) \right] \quad (1)$$

(Frank et al. 2002) to calculate $\Sigma(r, t)$ together with corresponding \dot{M}_{in} evolution. We use the α prescription of the kinematic viscosity, $\nu = \alpha c_s h$ (Shakura & Sunyaev 1973) where $h = c_s \Omega_K$ is the pressure scale height of the disk, $c_s = \sqrt{k_B T_c / \mu m_p}$ is the sound speed, m_p is the proton mass, μ is the mean molecular weight in units of m_p , and T_c is the mid-plane temperature of the disk. For a better resolution of the inner disk, we solve the diffusion equation substituting $x = 2r^{1/2}$ and $S = x\Sigma$ (Frank et al. 2002). We divide the disk into 800 radial grids equally spaced in x -space. Considering our assumption that all the inflowing disk matter is being accreted during the entire outburst phase, r_{in} should be taken equal to or smaller than r_{co} in the model. Nevertheless, the exact position of r_{in} between R_* and $r_{\text{co}} = 2.5R_*$ does

not affect \dot{M}_{in} evolution estimated from the solution of equation (1). For the numerical calculations, we take $r_{\text{in}} = r_{\text{co}}$, and allow all the inflowing matter to flow through the inner boundary freely (We take $\Sigma = 0$ at the inner disk edge). The outer disk is estimated to be cut by the strong tidal forces of the companion at a radius close to half of the Roche lobe radius (Frank et al. 2002), we set $r_{\text{out}} = 1.8 \times 10^{11}$ cm, which is about 60% of the Roche lobe radius. The exact value of r_{out} does not affect the model light curve either. For the numerical calculations, we neglect the tidal torques and assume that the matter flowing freely outward across the outer disk edge is lost from the system (We set $\Sigma = 0$ at $r = r_{\text{out}}$).

The viscous dissipation rate per unit disk area (from the mid-plane to the surface of the disk) can be written as

$$D(r) = \frac{9}{8} \nu \Sigma \frac{GM}{r^3} = \frac{4\sigma}{3\tau} T_c^4 \quad (2)$$

where σ Stephan-Boltzmann constant, and $\tau = \kappa \Sigma$ is the vertically integrated optical depth of the disk. For an optically thick, geometrically thin disk, $\tau \gg 1$, and the dissipated energy is emitted locally in the form of black-body radiation. We use the Rosseland mean opacities from the opacity tables for population I stars (Alexander & Ferguson 1994, for $\log T \leq 3.7$ and Iglesias & Rogers 1996, for $\log T > 3.7$).

In addition to viscous dissipation, the disk is also heated by the X-rays produced by the accretion onto the NS. The X-ray irradiation flux for a point source is given by

$$F_{\text{irr}} = \sigma T_{\text{irr}}^4 = \frac{\eta \dot{M}_* c^2 (1 - \epsilon)}{4\pi r^2} \frac{h}{r} \left(\frac{d \ln h}{d \ln r} - 1 \right) = C \frac{\dot{M}_* c^2}{4\pi r^2} \quad (3)$$

(Shakura & Sunyaev 1973; Dubus et al. 1999) where η is the efficiency of the conversion of rest mass energy into radiation and ϵ is the X-ray albedo of the disk surface, and

$$C \equiv \eta(1 - \epsilon) \frac{h}{r} \left(\frac{d \ln h}{d \ln r} - 1 \right) \quad (4)$$

is the irradiation parameter which is estimated to be in the range of $10^{-4} - 10^{-3}$ from the model fits to the optical and X-ray spectra of LMXBs (de Jong et al. 1996; Dubus et al. 1999; Ertan & Alpar 2002). Note that if F_{irr} is defined in terms of $L_X = \eta \dot{M}_* c^2$, then the irradiation parameter becomes greater than C given by equation (4) by a factor of $1/\eta$.

The effective temperature of the disk $T_{\text{eff}} \simeq [(D + F_{\text{irr}})/\sigma]^{1/4}$. At the inner disk regions, D dominates F_{irr} , while outside a radius ($\sim 10^9$ cm) the X-ray irradiation is the dominant heating mechanism. Since the h/r ratio in the equation (4) is not very sensitive

to \dot{M}_{in} and r ($h/r \propto \dot{M}_{\text{in}}^{3/20} r^{1/8}$), it seems reasonable to take C constant in the calculations (Frank et al. 2002). Nevertheless, in our simulations, we noticed that the variation of h/r with \dot{M}_{in} and the resultant change in F_{irr} significantly modify the slope of the X-ray light curve in the sharp decay phase after the knee. Including the weak \dot{M}_{in} and r dependence of h/r , equation (4) can be written as

$$C = C_0 \dot{M}_{\text{in},17}^{3/20} r_{10}^{1/8} \quad (5)$$

where $\dot{M}_{\text{in},17} = (\dot{M}_{\text{in}}/10^{17} \text{ g s}^{-1})$, $r_{10} = (r/10^{10} \text{ cm})$, and C_0 will be a free parameter of our model. We note that Lipunova et al. (2022) considered this dependence of the irradiation parameter on \dot{M}_{in} as well.

It was shown earlier through detailed analysis that the disk structure is not affected by the X-ray irradiation (Dubus et al. 1999; Lasota 2001). This means that the irradiation flux does not change the h/r ratio and its \dot{M}_{in} dependence along the hot portion of the disk. Nevertheless, the irradiation significantly affects the stability criteria of the disk by reducing the minimum critical surface densities for the transition to the cold state (King 1998; King & Ritter 1998; Dubus et al. 1999, 2001; Lasota 2001).

At the peak of the X-ray outburst, a large portion of the disk is irradiated. With decreasing L_X in the decay phase, the radius of the hot disk, r_h , decreases as well. The irradiation flux, F_{irr} , determines the current position of the hot disk radius, r_h , and governs the speed of its inward propagation. In this phase, the X-ray light curve characteristics are produced mainly by the dynamics of the hot inner disk. Meanwhile, the outer cold regions of the disk that remain outside r_h evolve with purely viscous decay, without any significant effect on the decay light curve. In other words, the \dot{M}_{in} dependence of the disk aspect ratio enters the model calculations across the hot disk only which could be approximated by a steady disk profile corresponding to the current mass-flow rate of the disk.

Following the conventional approach, we calculate the kinematic viscosity with two different α parameters, α_h and α_c , for the hot and cold viscosity states, respectively. For a given r in the cold (hot) state, there is a maximum (minimum) critical surface density Σ_{max} (Σ_{min}) for the transition to the hot (cold) state. We adopt Σ_{max} and Σ_{min} equations obtained by Dubus et al. (2001) through detailed vertical disk analyses. Interpolating the critical Σ values found for different radii of the disk, Dubus et al. (2001) obtained

$$\Sigma_{\text{max}} = (10.8 - 10.3 \xi) \alpha_c^{-0.84} M_1^{-0.37+0.1\xi} r_{10}^{1.11-0.27\xi} \text{ g cm}^{-2} \quad (6)$$

$$\Sigma_{\text{min}} = (8.3 - 7.1 \xi) \alpha_h^{-0.77} M_1^{-0.37} r_{10}^{1.12-0.23\xi} \text{ g cm}^{-2} \quad (7)$$

where $\xi = (T_{\text{irr}}/10^4 \text{ K})^2$, and M_1 is the mass of the NS in solar masses. For our initial mass distribution, $L_X \simeq 0$ until the surface densities increase at the inner disk, which is not realistic since L_X does not decrease below the quiescence level. Considering these situations, in addition to the critical surface densities, we also impose the $\alpha = \alpha_h$ condition for radii at which $T_{\text{eff}} > 6000 \text{ K}$, independent of T_{irr} .

The X-ray luminosity produced by accretion onto the star is related to the total disk luminosity through

$$L_{\text{acc}} \simeq \frac{GM\dot{M}_*}{R_*} \simeq \frac{2r_{\text{in}}}{R_*} L_{\text{disc}} \quad (8)$$

when r_{in} is not close to R_* . For the accretion onto the neutron star, r_{in} should be either equal to or smaller than r_{co} . For Aql X-1, $r_{\text{co}} = 2.5 \times 10^6 \text{ cm}$. For the numerical calculations, we take $r_{\text{in}} = r_{\text{co}}$. Nevertheless, our results do not change for $r_{\text{in}} < r_{\text{co}}$. For instance, if $r_{\text{in}} = R_*$, then the total X-ray luminosity $L_{\text{tot}} = GM\dot{M}_*/R_*$ and half of which is produced by the disk, mostly from the innermost disk regions. Here, we neglect the effects due to the fast rotation of Aql X-1, which depends on r_{in} (see e.g. Lipunova et al. 2022). The correction does not change our results by more than 25% for both $r_{\text{in}} = R_*$ and $r_{\text{in}} = r_{\text{co}}$ cases. For all our calculations, we take $M = 1.4M_{\odot}$ and $R_* = 1 \times 10^6 \text{ cm}$. During the transition to the propeller phase, L_X decreases rapidly by a factor greater than $\sim 2r_{\text{co}}/R_* \simeq 5$, since r_{in} should be greater than r_{co} in the propeller phase. Our results show that such a sharp modification of the model curve corresponding to accretion/propeller transition is not required to account for the observed outburst behavior of the source.

The maximum inner disk radius at which a steady propeller mechanism can be established could be written as

$$R_{\text{in,max}}^{25/8} |1 - R_{\text{in,max}}^{-3/2}| \simeq 1.26 \alpha_{-1}^{2/5} M_{1.4}^{-7/6} \dot{M}_{\text{in},16}^{-7/20} \mu_{30} P^{-13/12} \quad (9)$$

(Ertan 2017, 2018), where $R_{\text{in,max}} = r_{\text{in,max}}/r_{\text{co}}$, $M_{1.4} = (M/1.4M_{\odot})$, $\dot{M}_{\text{in},16} = (\dot{M}_{\text{in}}/10^{16} \text{ g s}^{-1})$, $\mu_{30} = (\mu/10^{30} \text{ G cm}^3)$, $\alpha_{-1} = (\alpha/0.1)$, and P is the spin period of the NS. Ertan (2017) derived this formula through analytical calculations adopting the basic results of the disk-magnetosphere interaction model proposed by Lovelace et al. (1995), which was developed later to simulate the propeller phase as well (Lovelace et al. 1999; Ustyugova et al. 2006). In this model, the inner disk settles down at a radius where the field lines can force the innermost disk matter into co-rotation. The inner disk-field interaction takes place in a narrow boundary with radial width $\Delta r < r$. The field lines interacting with matter inflate and open up within an interaction time-scale $\tau_{\text{int}} = |\Omega_K - \Omega_*|^{-1}$. In the propeller

phase, the matter can be thrown out along the open field lines. Subsequently, the lines reconnect on a time-scale similar to τ_{int} . The field lines outside the boundary are open and decoupled from the disk. With these conditions, Ertan (2017) found that the inflowing disk matter can be stopped at r_A , but cannot be thrown out from the system efficiently. The resultant pile-up pushes the inner disk inwards to the radius at which the field is strong enough to expel all the inflowing mass from the inner disk, continuously evacuating the inner boundary. Equation (9) gives the maximum radius at which this strong propeller condition is satisfied. In the propeller phase, $r_{\text{in}} = r_\eta$ does not scale with and in some cases significantly smaller than r_A (see Ertan 2017, 2018, 2021 for details).

The actual inner disk radius is estimated to be close to $r_{\text{in,max}}$, and can be written as $r_\eta = \eta r_{\text{in,max}}$ where η is a parameter close to unity. The L_X level corresponding to strong propeller/accretion transition can be estimated from equation (9). The predictions of this model for the critical L_X and the torque variations are in agreement with the properties of transitional millisecond pulsars (tMSPs; see Papitto & de Martino 2022 for a recent review) during their transitions between the LMXB and the radio millisecond pulsar (RMSP) states (Ertan 2017, 2018). The model was recently developed to include all the rotational phases of the NSs in LMXBs (Ertan 2018), and applied to the torque-reversal properties of LMXBs as well (Gençali et al. 2022). We use equation 9 to estimate the dipole field strength of Aql X-1 that is consistent with the results of our X-ray light curve analysis.

We also perform simulations to analyze and compare the repeating outburst light curves produced in the model with the observed recurrent outbursts of Aql X-1. To represent the mass flow from the companion, we add mass into the radial grid at r_{circ} at each time step. For Aql X-1, $r_{\text{co}} \simeq 2.5 \times 10^6$ cm, $r_{\text{circ}} = 5.0 \times 10^{10}$ cm, and we take $r_{\text{out}} = 1.8 \times 10^{11}$ cm in our calculations. We have repeated the numerical calculations with different mass-flow rates, \dot{M}_c , from the companion until we obtain typical outburst morphology and recurrence time of Aql X-1. In section 3, we discuss the results of the model calculations summarized above.

3. RESULTS AND DISCUSSION

3.1. The 2010 Outburst of Aql X-1

The model curve in Figure 1 is obtained with $\alpha_h = 0.1$, $\mu_h = 0.6$ in the hot state, and $\alpha_c = 5 \times 10^{-3}$, $\mu_c = 0.9$ in the cold state. The model can reproduce the basic features of the observed X-ray light curve with $C_0 \simeq 1.3 \times 10^{-4}$. The fluctuations seen in the decay phase

are not addressed in our model. Therefore, a seemingly good fit to data is sufficient for our purpose in this work. We note that the model curve represents the bolometric luminosity, while the observed luminosity is estimated from the 0.5–10 keV flux. As the temperature decreases during the decay phase (Campana et al. 2014), the bolometric correction factor also increases. For example, the gravitational redshift-corrected effective temperature at the onset of the sharp decay (1×10^{37} erg s $^{-1}$) is approximately 300 eV (Güngör et al. 2014), whereas during quiescence (5×10^{33} erg s $^{-1}$), it drops to 120 eV. We have estimated that the fraction of the total blackbody flux emitted in the observational band decreases from about 88% to 38%. This change does not significantly change the morphology of the light curve.

The sharp decay in L_X starts when r_h decreases to about 10^{10} cm. After the knee, the model cannot account for the functional form of the sharp decay curve without including the local \dot{M}_{in} dependence of the h/r ratio and its effect on F_{irr} . We smooth out the realistic opacities to prevent numerical fluctuations. The L_X fluctuations during the quiescent state are due to continuous mass flow toward the inner region of the cold outer disk and the resultant local instabilities continually taking part of this region into the hot state. We calculate the entire L_X curve with $\dot{M}_* = \dot{M}_{\text{in}}$. That is, L_X is produced by accretion onto the star without invoking any partial accretion or strong propeller. In this case, we can estimate an upper limit to the dipole field strength B on the surface of the star. Using equation (9) and the strong propeller condition $r_\eta > 1.26r_{\text{co}}$ (see Ertan 2021 for details), the \dot{M}_{in} level in the quiescent state ($\sim 1.5 \times 10^{14}$ g s $^{-1}$) gives $B < 4 \times 10^8$ G.

A model including the \dot{M}_{in} dependence of the disk aspect ratio in the F_{irr} calculation produces a much sharper decay curve after the knee in comparison with a model neglecting this dependence. Figure 1 shows the difference in the model curves obtained for these two cases.

How does a very weak \dot{M}_{in} and r dependence of h/r yield the difference in L_X curves seen in Figure 1? This can be understood by comparing hot disk radii, r'_h and r_h , obtained with constant and varying h/r , respectively. From equation 3, it can be shown that $r'_h \propto \dot{M}_{\text{in}}^{1/2}$. Using C given in equation 5, we obtain $r_h \propto \dot{M}_{\text{in}}^{46/75}$. During the decay phase, both r_h and r'_h decrease, while the r'_h/r_h ratio increases. Comparing the model curves in the bottom and upper panels of Figure 1, it is seen that $r_h \simeq r'_h$ when $L_X \simeq 10^{37}$ erg s $^{-1}$. With two orders decrease in L_X to $\sim 10^{35}$ erg s $^{-1}$, r'_h/r_h increases to 1.7.

It is the dynamics of the hot inner disk that determines the X-ray outburst light curve morphology. The mat-

ter at the outermost regions of the hot disk contributes to accretion onto the star after one viscous time across the disk. Relatively fast inward propagation of r_h also reduces the amount of hot matter more rapidly, which produces a cumulative effect leading to a sharper decline in L_X , and thus to an even faster shrinking size of the hot disk. For the case with constant C , the disk evolves with a larger hot disk size, that is, more matter flows to the star during the outburst state. This produces an outburst with relatively high L_X and long duration.

The model agrees with the observed L_X level in quiescence as well. The observed L_X is not smooth in quiescence. There are flares with ten-fold variations (Coti Zelati et al. 2014; Bernardini et al. 2013). These L_X fluctuations are also seen in our model curve. Nevertheless, correct modeling of this behavior is not easy due to the resolution problem for the innermost disk for a disk size greater than 10^{11} cm, which is beyond the scope of this work. We should also note that there are differences in the observed L_X levels after different outbursts (Campana et al. 2014).

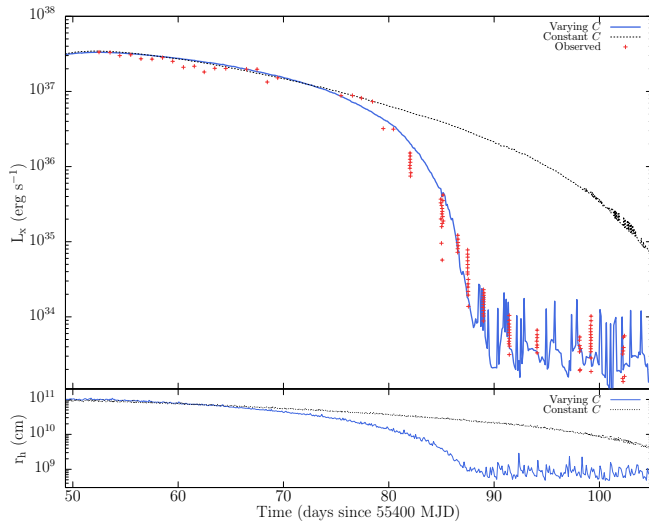


Figure 1. X-ray outburst light curve of Aql X-1 taken from Campana et al. (2014). The solid model curve is obtained with $\alpha_c = 5 \times 10^{-3}$, $\alpha_h = 0.1$, $\mu_c = 0.9$, $\mu_h = 0.6$, and $C_0 = 1.3 \times 10^{-4}$. For the L_X calculation, we take $\dot{M}_* = \dot{M}_{in}$ for the entire model curve. For comparison, the dotted curve is obtained with the same parameters, but with a constant irradiation parameter $C = 1.3 \times 10^{-4}$. The bottom panel shows the evolution of r_h (blue curve). For comparison r'_h (black curve) is also given.

3.2. The Quiescent State and Recurrent Outbursts

Using the same model parameters producing the model curve in Figure 1, we have continuously added mass into the radial grid at $r_{circ} = 5 \times 10^{10}$ cm to rep-

resent the mass flow into the outer disk from the companion. The outburst light curves seen in Figure 2 are obtained with $\dot{M}_c = 4 \times 10^{16}$ g s $^{-1}$ which produces outbursts with $\tau_{rec} \sim 1$ year. It is interesting that the model light curves of the second and fourth outbursts also seemingly fit well to the X-ray outburst data of Aql X-1. For instance, Figure 3 zooms in on the second outburst seen in Figure 2.

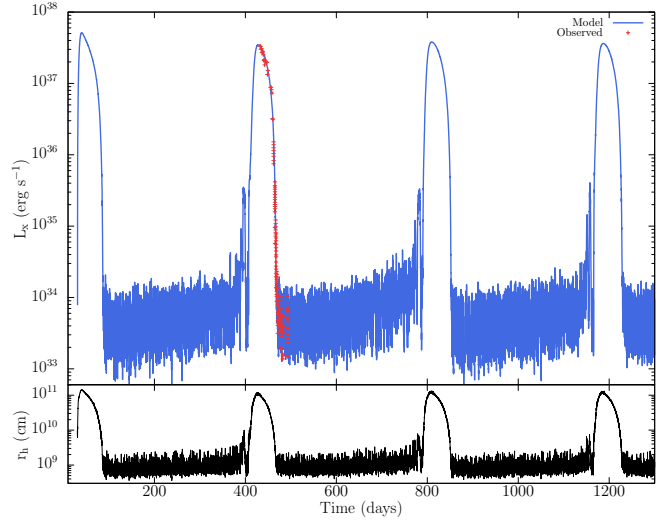


Figure 2. The same model parameters are used for the solid curve in Figure 1. This model curve is obtained by injecting mass into the radial grid at $r = r_{circ}$ with a rate of 4×10^{16} g s $^{-1}$. The recurrence time of the outbursts in this figure is enlarged in Figure 3. The bottom panel shows the evolution of the hot disk radius r_h .

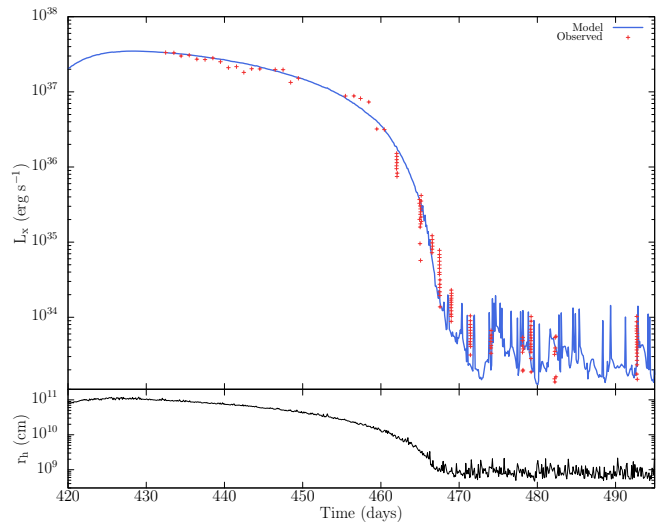


Figure 3. The second outburst seen in Figure 2. The bottom panel shows the evolution of the hot disk radius r_h .

For a comparison of our long-term ($\sim 10^4$ days) model light curve with the observations, we use the 2 – 10 keV data from the *All-Sky Monitor* (ASM) on the *Rossini X-ray Timing Explorer* and the *Monitor of All-sky X-ray Image* (MAXI) instrument mounted on the International Space Station (ISS). Count rates from these detectors are calibrated using the 2009 and 2010 outbursts which were observed by both instruments. In Figure 4, it is seen that the relative amplitudes and the recurrence time-scale of the outbursts produced in the model are very similar to the observed data. In the model, the recurrence time, relative amplitudes, and morphologies of the outbursts as well as the quiescent L_X level are sensitively depend on the α_c and \dot{M}_c parameters. The model curve in Figure 4 is obtained with $\alpha_c = 7.5 \times 10^{-3}$ and $\dot{M}_c = 4 \times 10^{16} \text{ g s}^{-1}$. Relatively high α_c produces outburst curves with higher quiescent L_X levels and relative amplitudes. For a given α_c , higher values of \dot{M}_c yield outbursts with smaller τ_{rec} . For instance, the model curves seen in Figures 3 and 5 are obtained with α_c values of 5×10^{-3} and 7.5×10^{-3} respectively. It is seen that the L_X level in the quiescent phase is a few times higher for the model with greater α_c . The data from the 2010 outburst were obtained in the energy range of 0.5–10 keV without bolometric correction. The blackbody temperature estimated from the spectral fits is about 120 eV in the quiescent state (Campana et al. 2014). This indicates a bolometric correction factor of ~ 2.7 in the quiescence, which means that the model with $\alpha_c = 7.5 \times 10^{-3}$ (Figure 5) is in better agreement with the corrected L_X level in the quiescent state.

The light curve morphologies of the recurrent outbursts seen in Figures 2 and 4 are not sensitive to the initial mass distribution in the model. Like the model with $\alpha_c = 5 \times 10^{-3}$, a fraction of the outburst model curves with $\alpha_c = 7.5 \times 10^{-3}$ naturally yields the morphology of the observed 2010 outburst light curve of Aql X-1. For instance, the model outburst given in Figure 5 is the same outburst indicated by an arrow in Figure 4. Indeed, there are observed outburst light curves of the source very similar to that of the 2010 outburst.

In the quiescent state of Aql X-1, $L_X \gtrsim 5 \times 10^{33} \text{ erg s}^{-1}$. For comparison, tMSPs are estimated to accrete matter from the disk down to L_X levels of $\sim 10^{33} \text{ erg s}^{-1}$ (Archibald et al. 2009; Papitto & de Martino 2022; Bassa et al. 2014). Below this level, X-ray pulses are switched off, and they show RMSP behavior. Dipole field strengths of tMSPs seem to be similar to that indicated by the upper limit $B < 4 \times 10^8 \text{ G}$ estimated for Aql X-1 in this work. Considering also the similarities in the rotational properties, Aql X-1 could have a critical \dot{M}_{in} rate for termination of accretion and

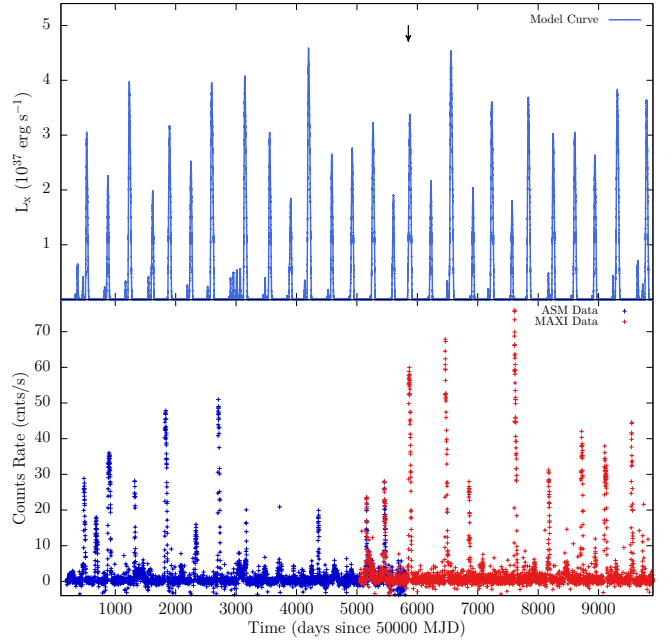


Figure 4. Top Panel: Long-term model light curve produced with $\alpha_c = 7.5 \times 10^{-3}$ and $\dot{M}_c = 4 \times 10^{16} \text{ g s}^{-1}$. The other parameters are the same as those given in Figure 1. Bottom Panel: The Long-term light curve of Aql X-1 from May 1996 to January 2023 observed by ASM(Blue) and MAXI(Red).

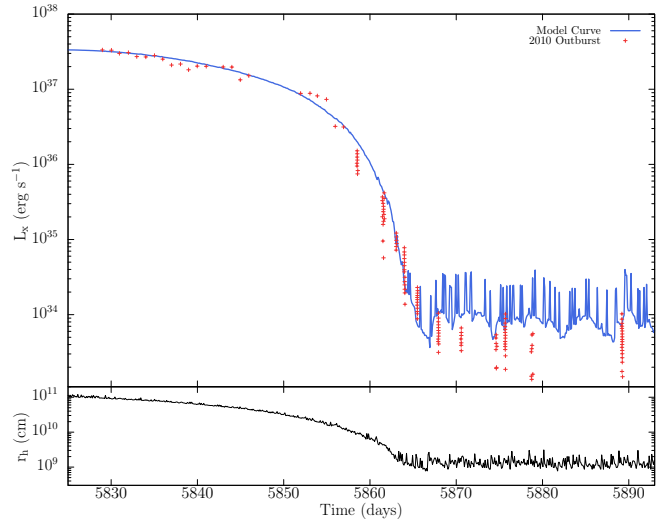


Figure 5. Enlarged model outburst curve shown by the arrow in Figure 4 (bolometric L_X). Red data points show the L_X curve estimated from the observed 0.5 – 10 keV flux data during the 2010 outburst of Aql X-1 for $d = 4.5 \text{ kpc}$ (Campana et al. 2014). The bottom panel shows the evolution of the hot disk radius r_h .

transition to the propeller phase that is similar to that of tMSPs. This might be the reason for the lack of radio pulsations from Aql X-1 during its quiescent state. It

is important to note here that the minimum pulsed L_X level of tMSPs is about two orders of magnitude smaller than the rate corresponding to $r_\xi = r_{\text{co}}$.

4. CONCLUSIONS

We have shown that the characteristic X-ray outburst light curve features of Aql X-1 can be reproduced by the mass accretion onto the neutron star along the entire X-ray outburst phase without requiring a transition into the propeller phase. The knee at the end of the initial slow exponential decay comes about as the cold/hot border of the disk approaches the inner disk, which is in line with the results obtained by Lipunova et al. (2022). The sharp decay phase after the knee can be accounted for by taking the weak \dot{M}_{in} and r dependence of the h/r ratio into account in the F_{irr} calculation. Throughout the outburst phase, we take $\dot{M}_{\text{in}} = \dot{M}_{\text{acc}}$ without including

any partial accretion regime or propeller effect in the L_X calculations. Injecting mass into the grid at r_{circ} with a rate of $\sim 4 \times 10^{16} \text{ g s}^{-1}$, the model can also generate recurrent X-ray outbursts that mimic typical outburst light curves of Aql X-1 consistently with the observed $\tau_{\text{rec}} \sim 1 \text{ yr}$. We have also estimated that $B < 4 \times 10^8 \text{ G}$ corresponding to $r_{\text{in}} \leq r_{\text{co}}$ for the lowest L_X level of the source.

We acknowledge research support from TÜBİTAK (The Scientific and Technological Research Council of Turkey) through grant 120F329 and from Sabancı University. We thank Ali Alpar for the useful comments that improved our manuscript. This research has made use of MAXI data provided by RIKEN, JAXA, and the MAXI team (Matsuoka et al. 2009) as well as results provided by the ASM/RXTE team.

REFERENCES

- Alexander, D. R., & Ferguson, J. W. 1994, *ApJ*, 437, 879, doi: [10.1086/175039](https://doi.org/10.1086/175039)
- Archibald, A. M., Stairs, I. H., Ransom, S. M., et al. 2009, *Science*, 324, 1411, doi: [10.1126/science.1172740](https://doi.org/10.1126/science.1172740)
- Bassa, C. G., Patruno, A., Hessels, J. W. T., et al. 2014, *MNRAS*, 441, 1825, doi: [10.1093/mnras/stu708](https://doi.org/10.1093/mnras/stu708)
- Bernardini, F., Cackett, E. M., Brown, E. F., et al. 2013, *MNRAS*, 436, 2465, doi: [10.1093/mnras/stt1741](https://doi.org/10.1093/mnras/stt1741)
- Campana, S., Brivio, F., Degenaar, N., et al. 2014, *MNRAS*, 441, 1984, doi: [10.1093/mnras/stu709](https://doi.org/10.1093/mnras/stu709)
- Campana, S., Coti Zelati, F., & D’Avanzo, P. 2013, *MNRAS*, 432, 1695, doi: [10.1093/mnras/stt604](https://doi.org/10.1093/mnras/stt604)
- Campana, S., Stella, L., Mereghetti, S., et al. 1998, *ApJL*, 499, L65, doi: [10.1086/311357](https://doi.org/10.1086/311357)
- Campana, S., Stella, L., Mereghetti, S., & de Martino, D. 2018, *A&A*, 610, A46, doi: [10.1051/0004-6361/201730769](https://doi.org/10.1051/0004-6361/201730769)
- Casella, P., Altamirano, D., Patruno, A., Wijnands, R., & van der Klis, M. 2008, *ApJL*, 674, L41, doi: [10.1086/528982](https://doi.org/10.1086/528982)
- Coti Zelati, F., Campana, S., D’Avanzo, P., & Melandri, A. 2014, *MNRAS*, 438, 2634, doi: [10.1093/mnras/stt2384](https://doi.org/10.1093/mnras/stt2384)
- Davidson, K., & Ostriker, J. P. 1973, *ApJ*, 179, 585, doi: [10.1086/151897](https://doi.org/10.1086/151897)
- de Jong, J. A., van Paradijs, J., & Augusteijn, T. 1996, *A&A*, 314, 484
- Dubus, G., Hameury, J. M., & Lasota, J. P. 2001, *A&A*, 373, 251, doi: [10.1051/0004-6361:20010632](https://doi.org/10.1051/0004-6361:20010632)
- Dubus, G., Lasota, J.-P., Hameury, J.-M., & Charles, P. 1999, *MNRAS*, 303, 139, doi: [10.1046/j.1365-8711.1999.02212.x](https://doi.org/10.1046/j.1365-8711.1999.02212.x)
- Ertan, Ü. 2017, *MNRAS*, 466, 175, doi: [10.1093/mnras/stw3131](https://doi.org/10.1093/mnras/stw3131)
- Ertan, Ü. 2018, *MNRAS*, 479, L12, doi: [10.1093/mnrasl/sly089](https://doi.org/10.1093/mnrasl/sly089)
- Ertan, Ü. 2021, *MNRAS*, 500, 2928, doi: [10.1093/mnras/staa3378](https://doi.org/10.1093/mnras/staa3378)
- Ertan, Ü., & Alpar, M. A. 2002, *A&A*, 393, 205, doi: [10.1051/0004-6361:20020998](https://doi.org/10.1051/0004-6361:20020998)
- Frank, J., King, A., & Raine, D. 2002, *Accretion Power in Astrophysics*, 3rd edn. (Cambridge University Press), doi: [10.1017/CBO9781139164245](https://doi.org/10.1017/CBO9781139164245)
- Gençali, A. A., Niang, N., Toyran, O., et al. 2022, *A&A*, 658, A13, doi: [10.1051/0004-6361/202141772](https://doi.org/10.1051/0004-6361/202141772)
- Ghosh, P., & Lamb, F. K. 1979, *ApJ*, 234, 296, doi: [10.1086/157498](https://doi.org/10.1086/157498)
- Güngör, C., Güver, T., & Ekşi, K. Y. 2014, *MNRAS*, 439, 2717, doi: [10.1093/mnras/stu128](https://doi.org/10.1093/mnras/stu128)
- Iglesias, C. A., & Rogers, F. J. 1996, *ApJ*, 464, 943, doi: [10.1086/177381](https://doi.org/10.1086/177381)
- Illarionov, A. F., & Sunyaev, R. A. 1975, *A&A*, 39, 185
- King, A. R. 1998, *MNRAS*, 296, L45, doi: [10.1046/j.1365-8711.1998.01652.x](https://doi.org/10.1046/j.1365-8711.1998.01652.x)
- King, A. R., & Ritter, H. 1998, *MNRAS*, 293, L42, doi: [10.1046/j.1365-8711.1998.01295.x](https://doi.org/10.1046/j.1365-8711.1998.01295.x)
- Kluźniak, W., & Rappaport, S. 2007, *ApJ*, 671, 1990, doi: [10.1086/522954](https://doi.org/10.1086/522954)
- Lamb, F. K., Pethick, C. J., & Pines, D. 1973, *ApJ*, 184, 271, doi: [10.1086/152325](https://doi.org/10.1086/152325)
- Lasota, J.-P. 2001, *NewAR*, 45, 449, doi: [10.1016/S1387-6473\(01\)00112-9](https://doi.org/10.1016/S1387-6473(01)00112-9)

- Lipunova, G., Malanchev, K., Tsygankov, S., et al. 2022, MNRAS, 510, 1837, doi: [10.1093/mnras/stab3343](https://doi.org/10.1093/mnras/stab3343)
- Lovelace, R. V. E., Romanova, M. M., & Bisnovatyi-Kogan, G. S. 1995, MNRAS, 275, 244, doi: [10.1093/mnras/275.2.244](https://doi.org/10.1093/mnras/275.2.244)
- Lovelace, R. V. E., Romanova, M. M., & Bisnovatyi-Kogan, G. S. 1999, ApJ, 514, 368, doi: [10.1086/306945](https://doi.org/10.1086/306945)
- Matsuoka, M., Kawasaki, K., Ueno, S., et al. 2009, PASJ, 61, 999, doi: [10.1093/pasj/61.5.999](https://doi.org/10.1093/pasj/61.5.999)
- Papitto, A., & de Martino, D. 2022, in Astrophysics and Space Science Library, Vol. 465, Astrophysics and Space Science Library, ed. S. Bhattacharyya, A. Papitto, & D. Bhattacharya, 157–200, doi: [10.1007/978-3-030-85198-9_6](https://doi.org/10.1007/978-3-030-85198-9_6)
- Psaltis, D. 2006, Accreting neutron stars and black holes: a decade of discoveries, ed. W. Lewin & M. van der Klis, Cambridge Astrophysics (Cambridge University Press), 1–38, doi: [10.1017/CBO9780511536281.002](https://doi.org/10.1017/CBO9780511536281.002)
- Shakura, N. I., & Sunyaev, R. A. 1973, A&A, 24, 337
- Ustyugova, G. V., Koldoba, A. V., Romanova, M. M., & Lovelace, R. V. E. 2006, ApJ, 646, 304, doi: [10.1086/503379](https://doi.org/10.1086/503379)
- van Paradijs, J. 1996, ApJL, 464, L139, doi: [10.1086/310100](https://doi.org/10.1086/310100)
- Zhang, S. N., Yu, W., & Zhang, W. 1998, ApJL, 494, L71, doi: [10.1086/311161](https://doi.org/10.1086/311161)